Advances in Nano Research, *Vol. 10, No. 5 (2021) 423-435*
DOI: https://doi.org/10.12989/anr.2021.10.5.423

Assessment of negative Poisson's ratio effect on thermal post-buckling of FG-GRMMC laminated cylindrical panels

Hui-Shen Shen*[1,2] and Y. Xiang[3]

[1]*School of Aeronautics and Astronautics, Shanghai Jiao Tong University, Shanghai 200240, People's Republic of China*
[2]*School of Ocean and Civil Engineering, Shanghai Jiao Tong University, Shanghai 200240, People's Republic of China*
[3]*School of Engineering, Design and Built Environment, Western Sydney University, Locked Bag 1797, Penrith, NSW 2751, Australia*

(*Received December 23, 2020, Revised January 9, 2021, Accepted January 10, 2021*)

Abstract. This paper examines the thermal post-buckling behaviors of graphene-reinforced metal matrix composite (GRMMC) laminated cylindrical panels which possess in-plane negative Poisson's ratio (NPR) and rest on an elastic foundation. A panel consists of GRMMC layers of piece-wise varying graphene volume fractions to obtain functionally graded (FG) patterns. Based on the MD simulation results, the GRMMCs exhibit in-plane NPR as well as temperature-dependent material properties. The governing equations for the thermal post-buckling of panels are based on the Reddy's third order shear deformation shell theory. The von Kármán nonlinear strain-displacement relationship and the elastic foundation are also included. The nonlinear partial differential equations for GRMMC laminated cylindrical panels are solved by means of a singular perturbation technique in associate with a two-step perturbation approach and in the solution process the boundary layer effect is considered. The results of numerical investigations reveal that the thermal post-buckling strength for $(0/90)_{5T}$ GRMMC laminated cylindrical panels can be enhanced with an FG-X pattern. The thermal post-buckling load-deflection curve of 6-layer $(0/90/0)_S$ and $(0/90)_{3T}$ panels of FG-X pattern are higher than those of 10-layer $(0/90/0/90/0)_S$ and $(0/90)_{5T}$ panels of FG-X pattern.

Keywords: auxetic materials; temperature-dependent; functionally graded; cylindrical panels; thermal post-buckling; elastic foundation

1. Introduction

It is well known that conventional materials experience expansion when compressed. This trend is reversed for the so-called auxetic materials in which contraction is observed when compressed which enables the materials to possess negative Poisson's ratio (NPR). Due to this exotic characteristics, auxetic materials can perform better in certain circumstances than the conventional materials, e.g. indentation resistance, fracture resistance, energy absorption, etc. (Liu 2006, Prawoto 2012, Mir *et al*. 2014, Huang and Chen 2016, Saxena *et al*. 2016, Lakes 2017, Ren *et al*. 2018). One of the potential applications of such materials is to create auxetic honeycomb core sandwich structures (Duc *et al*. 2017, Cong *et al*. 2018, Duc and Cong 2018, Zhang *et al*. 2019). Recently, a series of studies were conducted by Li *et al*. (2019a, b, c, d, 2020a, b, c, d) on the nonlinear mechanical behaviors, i.e., large amplitude vibration, nonlinear bending and post-buckling, for auxetic honeycomb sandwich beams and plates subject to different loading and thermal conditions. The results from their studies revealed that sandwich plates with NPR core can have substantially higher thermal post-buckling temperatures when comparing with their counterparts with positive Poisson's ratio core (Li *et al*. 2020a).

Another way to obtain NPR in laminates is by arranging the stacking sequence of the laminated layers and orientation angles in certain patterns (Herakovich 1984, Milton 1992, Clarke *et al*. 1994, Hine *et al*. 1997, Zhang *et al*. 1998, Yeh and Yeh 1999, Evans *et al*. 2004, Harkati *et al*. 2007). It is revealed that higher NPR values can be obtained when the carbon fiber reinforced laminate is strong anisotropy (Sun and Li 1988). However, the effect of NPR on the mechanical responses of auxetic laminated structures is scarce. In this regard, Alderson and Coenen (2008) studied the response of auxetic carbon fiber reinforced $(\pm 30)_{6S}$ laminates with out-of-plane NPR ν_{13} = -0.156 subject to low velocity impact. The influence of out-of-plane NPR on the vibration behavior of a 5-layered composite beam with two embedded auxetic layers was investigated by Azoti *et al*. (2013). The nonlinear dynamic responses for a laminated plate having two auxetic layers were reported by Chen and Feng (2017) where the NPR was assumed to be in the range of -0.3 to -0.9 which was not directly related to available real composite materials.

Functionally graded (FG) materials with inhomogeneous elastic properties have recently been used in a variety of engineering sectors including mechanical, aerospace, electronics, biomedical, chemical and nuclear engineering (Shen 2009a). Shen (2009b) first proposed FG carbon nanotube reinforced composites (CNTRCs) and then extended to the FG-CNTRC laminates with NPR (Shen *et al*. 2020a) due to the high ratio value of the two in-plane Young's moduli (E_{11}/E_{22} > 40) of CNTRC laminates. The

*Corresponding author, Professor,
E-mail: hsshen@sjtu.edu.cn

ISSN: 2287-237X (Print), 2287-2388 (Online)

effect of out-of-plane NPR on the nonlinear bending behaviors and nonlinear vibration characteristics of CNTRC plates and beams was examined by Shen *et al*. (2020b), Yang *et al*. (2020a, b, c) and Yu and Shen (2020a, b). The dynamic responses of FG-CNTRC laminated beams and plates with out-of-plane NPR were then studied by Fan and Wang (2021) and Huang *et al*. (2020a, b).

Shell panels are a type of structural components encountered in many engineering fields. When comparing with flat plates, shell panels are stiffer and can be used as light weight structural components or where large span/clearance is required. When subjected to high temperature, composite panels can buckle due to thermal loading (Karami and Karami 2019, Ebrahimi *et al*. 2019, Mehar and Panda 2019). Many research works were reported in open literature on thermal post-buckling responses for cylindrical panels made of fiber reinforced composites (FRCs) and CNTRCs subject to elevated temperature (Oh and Lee 2001, Lee *et al*. 2002, Roh *et al*. 2004, Panda and Singh 2009, 2013, Lal *et al*. 2012, Shen and Xiang 2015, Trang and Tung 2020). The results revealed that the thermal post-buckling equilibrium path is not the bifurcation-type for a laminated cylindrical panel with simply supported boundary condition and immovable in-plane edge constraint. This is mainly due to the existence of initial deflection in the panel. There are two reasons for the initial deflection. Firstly, the initial deflection is caused by compressive stress on the two immovable straight edges of the panel under elevated temperature. Secondly, the initial deflection may be caused by thermal bending if the panel is asymmetric.

Graphene is a two-dimensional material of extraordinary characteristics in the carbon family (Novoselov *et al*. 2004) which possesses anisotropic (Ni *et al*. 2010) and temperature dependent (Shen *et al*. 2010) material properties and may also have in-plane NPR (Fan *et al*. 2019). Using molecular dynamics simulations, a complete set of material properties of PMMA based graphene reinforced composites (GRCs) was obtained by Lin *et al*. (2017). Subsequently, Shen *et al*. (2017a, b, 2019b) and Shen and Xiang (2019) investigated the thermal post-buckling responses of FG-GRC laminated structures. Thermal post-buckling studies for FG-GRC laminated structures were also carried out by Mirzaei and Kiani (2017), Kiani (2018), and Kiani, and Mirzaei (2018) using the finite element method.

The major disadvantage of polymer matrix composite structures is their inability to withstand high temperature, while metal matrix composite (MMC) structures can enhance temperature resistance of the structures. Our literature survey has revealed that studies on the thermal buckling responses of MMC laminated structures are scarce. Among a few reported researches in this area, Paley and Aboudi (1991), and Feldman and Aboudi (1995) studied the inelastic thermal buckling and post-buckling of MMC antisymmetric laminated plates including viscoplastic effect. The same problem for the inelastic thermal buckling of MMC symmetric laminated plates under non-uniform thermal loading was performed by Feldman (1996). Shen and Wang (2013) investigated the thermal post-buckling behaviors of anisotropic laminated MMC cylindrical shells subject to a uniform temperature rise. On the other hand, Dehrouyeh-Semnani and Jafarpour (2019) carried out the thermal post-buckling analysis of laminated MMC shallow arches under thermal loading.

With the development of material science, metal matrix reinforced by graphene fillers has emerged as a new type of advanced nanocomposites (Hu *et al*. 2016, Dadkhah *et al*. 2019, Naseer *et al*. 2019, Tabandeh-Khorshid *et al*. 2020) in recent years. Using molecular dynamics simulations, Fan *et al*. (2020) obtained a set of temperature-dependent material properties of GRMMC using single crystalline copper (Cu) as the matrix and observed for the first time that the graphene/Cu composite exhibits auxetic behavior in the in-plane directions. Based on the GRMMC material properties from Fan *et al*. (2020), Shen *et al*. (2020c) and Shen and Xiang (2020) investigated the compressive post-buckling responses for GRMMC laminated flat and cylindrical panels with the effect of in-plane NPR.

The aim of this work is to examine the thermal buckling and post-buckling behaviors of auxetic GRMMC laminated cylindrical panels resting on an elastic foundation and subject to a uniform temperature rise. For the GRMMC panel, the in-plane NPR is achieved due to the auxetic GRMMC layers and the arrangement of the GRMMC layers with special orientation angles and stacking sequence. The graphene sheets are aligned (Liang *et al*. 2011) and the FG patterns of the panels can be formed by arranging the GRMMC layers with piece-wise varying volume fractions of graphene fillers. The thermo-mechanical properties of GRMMC are temperature-dependent. The Reddy's third order shear deformation shell theory is utilized to obtain the governing equations for the FG-GRMMC laminated cylindrical panels. The geometric nonlinearity in the von Kármán sense, temperature variation and initial geometric imperfection are included in deriving the governing equations. Applying the singular perturbation technique in associate with a two-step perturbation approach, the thermal post-buckling problem is solved and thermal post-buckling load-deflection curves are obtained for the auxetic GRMMC laminated cylindrical panels.

2. Modelling of FG-GRMMC laminated cylindrical panels

Fig. 1 shows a cylindrical panel resting on an elastic foundation and having a coordinate system (X, Y, Z) with its origin being located at the corner on the mid-plane, where X, Y and Z are the axes in the longitudinal, the circumferential and the inward normal to middle plane directions, respectively. The panel is of total thickness h, axial length a, circumferential length b and radius R and consists of N GRMMC layers of the same thickness. The piece-wise FG patterns of the panel are achieved by arranging the GRMMC layers having different values of graphene volume fraction cross the panel thickness. An arithmetic series of 0.05, 0.07, 0.09, 0.11 and 0.13 of graphene volume fractions (Fan *et al*. 2020) is selected for multilayered GRMMC laminated cylindrical panels.

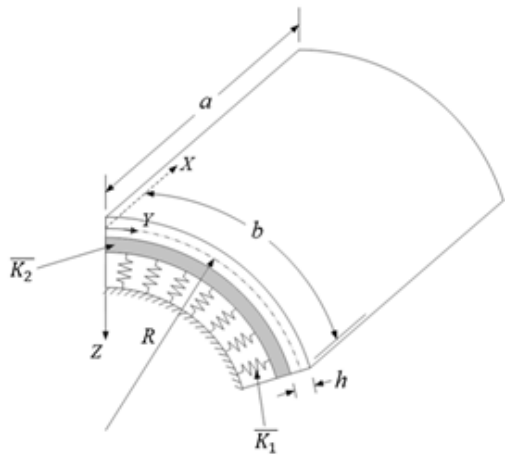

Fig. 1 Geometry and coordinate system for a GRMMC cylindrical panel rested on a Pasternak foundation

Sharma *et al*. (2017) reported that up to 16% graphene volume fraction can be achieved in GRMMCs, while we apply up to 13% graphene volume fraction in GRMMC layers in the current study. Cylindrical panels of ten GRMMC layers with four different FG patterns are considered in the current study which are named as FG-Λ ($[(0.05)_2/(0.07)_2/(0.09)_2/(0.11)_2/(0.13)_2]$), FG-V ($[(0.13)_2/(0.11)_2/(0.09)_2/(0.07)_2/(0.05)_2]$), FG-O ($[0.05/0.07/0.09/0.11/0.13]_S$) and FG-X ($[0.13/0.11/0.09/0.07/0.05]_S$), respectively. For comparison purpose, we also consider a UD laminated cylindrical panel with ten GRMMC layers of the same graphene volume fraction ($[(0.09)_{10}]$).

Due to their temperature resistance property, GRMMCs are ideal for applications in high temperature environment (Tabandeh-Khorshid *et al*. 2020). For a novel class of advanced materials, one important aspect is to predict the thermal-mechanical properties of GRMMCs firstly when studying the thermal post-buckling of GRMMC laminated panels. As mentioned previously (Shen *et al*. 2020c, Shen and Xiang 2020), the negative Poisson's ratio ν_{12} and the thermal expansion coefficients α_{11} and α_{21} of the GRMMC layer are far different from that predicted by any conventional micromechanical model. In the current study, the thermal-mechanical properties of GRMMCs are expressed as a nonlinear function of temperature based on the MD simulation results of Fan *et al*. (2020) as

$$P_f = P_0 + P_1 T + P_2 T^2 + P_3 T^3 \tag{1}$$

where the coefficients associated with temperature T (K) are P_0, P_1, P_2 and P_3 which are unique to the GRMMC layers.

The panel is rested on a Pasternak foundation with stiffness $\bar{K}_1$ for the vertical spring and stiffness $\bar{K}_2$ for the shearing layer. The panel-foundation interactive force p_0 is given by $p_0 = \bar{K}_1\bar{W} - \bar{K}_2\nabla^2\bar{W}$, where the displacement $\bar{W}$ is in the Z direction, and the Laplace operator ∇^2 is related to the coordinate variables X and Y.

The panel is in a thermal environment with uniformly elevated temperature. We employ the Reddy's third order shear deformation shell theory (Reddy and Li 1985) to model the auxetic GRMMC laminated cylindrical panel. The von Kármán geometric nonlinearity, foundation support and thermal effect are considered in the modeling. The governing equations for the panel may be given by

$$\begin{bmatrix} \tilde{L}_{11}() + \bar{K}_1() - \bar{K}_2\nabla^2() & -\tilde{L}_{12}() & -\tilde{L}_{13}() & \tilde{L}_{14}() - \frac{1}{R}\frac{\partial^2()}{\partial X^2} \\ -\tilde{L}_{24}() + \frac{1}{R}\frac{\partial^2()}{\partial X^2} & \tilde{L}_{22}() & \tilde{L}_{23}() & \tilde{L}_{21}() \\ \tilde{L}_{31}() & \tilde{L}_{32}() & \tilde{L}_{33}() & \tilde{L}_{34}() \\ \tilde{L}_{41}() & \tilde{L}_{42}() & \tilde{L}_{43}() & \tilde{L}_{44}() \end{bmatrix} \begin{bmatrix} \bar{W} \\ \bar{\Psi}_x \\ \bar{\Psi}_y \\ \bar{F} \end{bmatrix} - \begin{bmatrix} \tilde{L}_{15}() & \tilde{L}_{16}() & 0 & 0 \\ \tilde{L}_{25}() & 0 & 0 & 0 \\ \tilde{L}_{35}() & 0 & \tilde{L}_{36}() & 0 \\ \tilde{L}_{45}() & 0 & 0 & \tilde{L}_{46}() \end{bmatrix} \begin{bmatrix} \bar{N}^T \\ \bar{M}^T \\ \bar{S}^T \\ \bar{S}^T \end{bmatrix} = \begin{bmatrix} \tilde{L}(\bar{W} + \bar{W}^*, \bar{F}) \\ -\frac{1}{2}\tilde{L}(\bar{W} + 2\bar{W}^*, \bar{W}) \\ 0 \\ 0 \end{bmatrix} \tag{2}$$

where $\bar{W}^*$ is the additional deflection of the panel caused by the initial geometric imperfection, and $\bar{\Psi}_x$ and $\bar{\Psi}_y$ represent the rotations about the Y and X axes, and the stress function $\bar{F}$ is defined by $\bar{N}_x = \partial^2\bar{F}/\partial Y^2$, $\bar{N}_y = \partial^2\bar{F}/\partial X^2$ and $\bar{N}_{xy} = -\partial^2\bar{F}/\partial X\partial Y$. $\tilde{L}_{ij}()$ are linear operators which have been defined in Shen (2017). The nonlinear operator $\tilde{L}()$ can be written as

$$\tilde{L}() = \frac{\partial^2}{\partial X^2}\frac{\partial^2}{\partial Y^2} - 2\frac{\partial^2}{\partial X\partial Y}\frac{\partial^2}{\partial X\partial Y} + \frac{\partial^2}{\partial Y^2}\frac{\partial^2}{\partial X^2} \tag{3}$$

Eq. (2) includes the foundation effect through the terms relating to the foundation stiffnesses $\bar{K}_1$ and $\bar{K}_2$. The terms with superscript T in Eq. (2) are relating to the temperature effect. Note that the effect of temperature is also included in the GRMMC material properties. $\bar{N}^T$, $\bar{M}^T$ and $\bar{S}^T$ caused by temperature rise are given in Appendix A.

The panel's two straight edges are simply supported (S) while its two curved edges are assumed to be either simply supported (S) or clamped (C). Note that all edges are constrained against in-plane displacements. The boundary conditions of the SSSS panel can be given as

$$\bar{W} = \bar{\Psi}_y = \bar{M}_x = \bar{P}_x = 0 \ \ (\text{at } X = 0, a) \tag{4a}$$

$$\bar{W} = \bar{\Psi}_x = \bar{M}_y = \bar{P}_y = 0 \ \ (\text{at } Y = 0, b) \tag{4b}$$

and for the CSCS panel, they are

$$\bar{W} = \bar{\Psi}_x = \bar{\Psi}_y = 0 \ (\text{at } X = 0, a) \tag{5a}$$

$$\bar{W} = \bar{\Psi}_x = \bar{M}_y = \bar{P}_y = 0 \ (\text{at } Y = 0, b) \tag{5b}$$

where $\bar{M}_x$ and $\bar{M}_y$ denote the bending moments, and $\bar{P}_x$ and $\bar{P}_y$ denote the higher order moments as given in Reddy and Li (1985).

Unlike compressive post-buckling problem of the panel where the displacement in the axial direction should be movable (Shen and Xiang 2020), in the current study, the in-plane boundary conditions are immovable and can be written as

$$\bar{U} = 0 \ (\text{at } X = 0, a) \tag{6a}$$

$$\bar{V} = 0 \ (\text{at } Y = 0, b) \tag{6b}$$

and they may be fulfilled in the average sense as

$$\int_0^b \int_0^a \frac{\partial \bar{U}}{\partial X} dX dY = 0, \quad \int_0^a \int_0^b \frac{\partial \bar{V}}{\partial Y} dY dX = 0 \tag{7a}$$

which yields

$$\int_0^b\int_0^a\left[A_{11}^*\frac{\partial^2\bar{F}}{\partial Y^2}+A_{12}^*\frac{\partial^2\bar{F}}{\partial X^2}+\left(B_{11}^*-\frac{4}{3h^2}E_{11}^*\right)\frac{\partial\bar{\Psi}_x}{\partial X}+\left(B_{12}^*-\frac{4}{3h^2}E_{12}^*\right)\frac{\partial\bar{\Psi}_y}{\partial Y}-\frac{1}{2}\left(\frac{\partial\bar{W}}{\partial X}\right)^2-\frac{\partial\bar{W}}{\partial X}\frac{\partial\bar{W}^*}{\partial X}-(A_{11}^*\bar{N}_x^T+A_{12}^*\bar{N}_y^T)\right]dXdY=0 \tag{8a}$$

$$\int_0^a\int_0^b\left[A_{22}^*\frac{\partial^2\bar{F}}{\partial X^2}+A_{12}^*\frac{\partial^2\bar{F}}{\partial Y^2}+\left(B_{21}^*-\frac{4}{3h^2}E_{21}^*\right)\frac{\partial\bar{\Psi}_x}{\partial X}+\left(B_{22}^*-\frac{4}{3h^2}E_{22}^*\right)\frac{\partial\bar{\Psi}_y}{\partial Y}-\frac{4}{3h^2}\left(E_{21}^*\frac{\partial^2\bar{W}}{\partial X^2}+E_{22}^*\frac{\partial^2\bar{W}}{\partial Y^2}\right)+\frac{\bar{W}}{R}-\frac{1}{2}\left(\frac{\partial\bar{W}}{\partial Y}\right)^2-\frac{\partial\bar{W}}{\partial Y}\frac{\partial\bar{W}^*}{\partial Y}-(A_{12}^*\bar{N}_x^T+A_{22}^*\bar{N}_y^T)\right]dYdX=0 \tag{8b}$$

where the reduced stiffness matrices of the panel $[A_{ij}^*]$, $[B_{ij}^*]$, etc. are given in Appendix B.

3. Solution procedure

It was reported by Shen (2017) that the boundary layer effect must be considered for the accurate analysis of thermal post-buckling of cylindrical panels subject to thermal loading. The boundary layer effect is taken into consideration in the current study by first transforming the governin Eq. (2) to the boundary layer type equation as

$$\begin{bmatrix}\varepsilon^2[L_{11}()+K_1(\,)-K_2\nabla^2(\,)] & -\varepsilon L_{12}() & -\varepsilon L_{13}() & \varepsilon\gamma_{14}L_{14}()-\gamma_{14}\dfrac{\partial^2()}{\partial x^2}\\ -\varepsilon\gamma_{24}L_{24}()+\gamma_{24}\dfrac{\partial^2()}{\partial x^2} & \gamma_{24}L_{22}() & \gamma_{24}L_{23}() & L_{21}()\\ \varepsilon L_{31}() & L_{32}() & L_{33}() & \gamma_{14}L_{34}()\\ \varepsilon L_{41}() & L_{42}() & L_{43}() & \gamma_{14}L_{44}()\end{bmatrix}\begin{bmatrix}W\\ \Psi_x\\ \Psi_y\\ F\end{bmatrix}-\begin{bmatrix}0 & \varepsilon L_{16}() & 0 & 0\\ 0 & 0 & 0 & 0\\ 0 & 0 & \varepsilon L_{36}() & 0\\ 0 & 0 & 0 & \varepsilon L_{46}()\end{bmatrix}\begin{bmatrix}N^T\\ M^T\\ S^T\\ S^T\end{bmatrix}=\begin{bmatrix}\gamma_{14}\beta^2L(W+W_T^*,F)\\ -\frac{1}{2}\gamma_{24}\beta^2L(W+2W_T^*,W)\\ 0\\ 0\end{bmatrix} \tag{9}$$

where $W_T^*=W^*+W_I^*+W_{II}^*$, consisting of the additional thermal deflection W_I^* and the additional deflection W_{II}^* due to compressive stresses caused by the immovable edges. Note that $W_I^*=0$ when $\Delta T=0$. $L_{ij}(\,)$ and $L(\,)$ are non-dimensional operators and are derived in Shen (2017). Evidently, when $\varepsilon<1$, Eq. (9) becomes the boundary layer type equation that contains panel initial geometric imperfections, pre-buckling deformations and large deflections in the post-buckling domain, simultaneously. The dimensionless parameters in Eq. (9) are given as follows

$$\begin{aligned}&x=\pi\frac{X}{a},\qquad y=\pi\frac{Y}{b},\qquad \beta=\frac{a}{b},\\ &\varepsilon=\frac{\pi^2R}{a^2}[D_{11}^*D_{22}^*A_{11}^*A_{22}^*]^{\frac{1}{4}},\qquad \bar{Z}=\frac{a^2}{Rh},\\ &(W,W^*)=\varepsilon\frac{(\bar{W},\bar{W}^*)}{[D_{11}^*D_{22}^*A_{11}^*A_{22}^*]^{\frac{1}{4}}},\\ &(\Psi_x,\Psi_y)=\varepsilon^2\frac{a}{\pi}\frac{(\bar{\Psi}_x,\bar{\Psi}_y)}{[D_{11}^*D_{22}^*A_{11}^*A_{22}^*]^{\frac{1}{4}}},\quad F=\varepsilon^2\frac{\bar{F}}{[D_{11}^*D_{22}^*]^{\frac{1}{2}}},\\ &(M_x,\ P_x)=\varepsilon^2\frac{a^2}{\pi^2}\frac{1}{D_{11}^*[D_{11}^*D_{22}^*A_{11}^*A_{22}^*]^{\frac{1}{4}}}\left(\bar{M}_x,\ \frac{4}{3h^2}\bar{P}_x\right),\\ &\gamma_{14}=\left[\frac{D_{22}^*}{D_{11}^*}\right]^{\frac{1}{2}},\quad \gamma_{24}=\left[\frac{A_{11}^*}{A_{22}^*}\right]^{\frac{1}{2}},\quad \gamma_5=-\frac{A_{12}^*}{A_{22}^*},\end{aligned} \tag{10}$$

$$\begin{aligned}&(\gamma_{T1},\gamma_{T2})=(A_x^T,\ A_y^T)R\left[\frac{A_{11}^*A_{22}^*}{D_{11}^*D_{22}^*}\right]^{\frac{1}{4}},\\ &(\gamma_{T4},\gamma_{T5},\gamma_{T7},\gamma_{T8})=\frac{a^2}{\pi^2hD_{11}^*}\left(D_x^T,\ D_y^T,\ \frac{4}{3h^2}F_x^T,\ \frac{4}{3h^2}F_y^T\right),\\ &(K_1,k_1)=\bar{K}_1\left(\frac{a^4}{\pi^4D_{11}^*},\ \frac{b^4}{E_0h^3}\right),\\ &(K_2,k_2)=\bar{K}_2\left(\frac{a^2}{\pi^2D_{11}^*},\ \frac{b^2}{E_0h^3}\right),\qquad \lambda_T=\alpha_0\Delta T,\end{aligned}$$

in which E_0 is E_{22} for the UD GRMMC laminated cylindrical panel with T_0 = 300 K, k_1 and k_2 are dimensionless foundation parameters, and A_x^T, A_y^T, etc., are defined by

$$\begin{bmatrix}A_x^T & D_x^T & F_x^T\\ A_y^T & D_y^T & F_y^T\end{bmatrix}\Delta T=-\sum_{k=1}^{N}\int_{h_{k-1}}^{h_k}\begin{bmatrix}A_x\\ A_y\end{bmatrix}_k(1,Z,Z^3)\Delta T dZ \tag{11}$$

The boundary conditions for the SSSS panel become

$$W=\Psi_y=M_x=P_x=0\qquad(\text{at } x=0,\ \pi) \tag{12a}$$

$$W=\Psi_x=M_y=P_y=0\qquad(\text{at } y=0,\ \pi) \tag{12b}$$

and for the CSCS panel, they become

$$W=\Psi_x=\Psi_y=0\qquad(\text{at } x=0,\ \pi) \tag{13a}$$

$$W=\Psi_x=M_y=P_y=0\qquad(\text{at } y=0,\ \pi) \tag{13b}$$

and the in-plane immovable conditions of Eqs. (8a) and (8b) become

$$\int_0^\pi\int_0^\pi\left[\left(\gamma_{24}^2\beta^2\frac{\partial^2F}{\partial y^2}-\gamma_5\frac{\partial^2F}{\partial x^2}\right)+\gamma_{24}\left(\gamma_{511}\frac{\partial\Psi_x}{\partial x}+\gamma_{233}\beta\frac{\partial\Psi_y}{\partial y}\right)-\varepsilon\gamma_{24}\left(\gamma_{611}\frac{\partial^2W}{\partial x^2}+\gamma_{244}\beta^2\frac{\partial^2W}{\partial y^2}\right)-\frac{1}{2}\gamma_{24}\left(\frac{\partial W}{\partial x}\right)^2-\gamma_{24}\frac{\partial W}{\partial x}\frac{\partial W_T^*}{\partial x}+\varepsilon(\gamma_{24}^2\gamma_{T1}-\gamma_5\gamma_{T2})\lambda_T\right]dxdy=0 \tag{14a}$$

$$\int_0^\pi\int_0^\pi\left[\left(\frac{\partial^2F}{\partial x^2}-\gamma_5\beta^2\frac{\partial^2F}{\partial y^2}\right)+\gamma_{24}\left(\gamma_{220}\frac{\partial\Psi_x}{\partial x}+\gamma_{522}\beta\frac{\partial\Psi_y}{\partial y}\right)-\varepsilon\gamma_{24}\left(\gamma_{240}\frac{\partial^2W}{\partial x^2}+\gamma_{622}\beta^2\frac{\partial^2W}{\partial y^2}\right)+\gamma_{24}W-\frac{1}{2}\gamma_{24}\beta^2\left(\frac{\partial W}{\partial y}\right)^2-\gamma_{24}\beta^2\frac{\partial W}{\partial y}\frac{\partial W_T^*}{\partial y}+\varepsilon(\gamma_{T_2}-\gamma_5\gamma_{T1})\lambda_T\right]dydx=0 \tag{14b}$$

The total initial deflection of the panel may be expressed by

$$W_T^*(x,y,\varepsilon)=\varepsilon\mu A_{11}^{(2)}\sin m\,x\sin n\,y \tag{15}$$

where μ is the imperfection parameter.

The solution procedure is carried out by means of a singular perturbation technique in associate with a two-step perturbation approach which was developed by Shen (2013) and was applied by many researchers to solve various nonlinear boundary value problems of curved panels successfully (She *et al*. 2017, Sahmani and Fattahi 2017a, b, Babaei *et al*. 2018, 2019, Zhao *et al*. 2018, Bayat and Mashhadi 2018, Ma *et al*. 2019). We can separate Eq. (9) into two sets of equations and then first obtain W_I^* caused by rising temperature. Afterwards, the thermal post-buckling problem of auxetic GRMMC laminated cylindrical panels was solved by employing the two-step perturbation approach. The displacements W, Ψ_x and Ψ_y, and the stress

function F can be determined in two parts, i.e., the regular solutions combined with the boundary layer solutions where the boundary layer variables at the vicinity of the panel's two curved ends are defined by $\xi = x/\varepsilon^{1/2}$ and $\zeta = (\pi - x)/\varepsilon^{1/2}$. By matching the regular and the boundary layer solutions at the panel's curved ends, we can obtain the solutions for W, Ψ_x, Ψ_y and F (as shown in Appendix B). It is worth noting that the higher order perturbation solution is not necessarily more correct than the lower order solution, as previously pointed out in Shen *et al.* (2019a). From Eq. (B.1), the present solution shows that the pre-buckling deformation is nonlinear. Finally, the thermal post-buckling solutions for the auxetic GRMMC panel can be obtained as

$$\lambda_T = C_{11}[\lambda_T^{(0)} - \lambda_T^{(2)}(A_{11}^{(2)}\varepsilon)^2 + \lambda_T^{(4)}(A_{11}^{(2)}\varepsilon)^4 + \cdots] \quad (16)$$

in which $(A_{11}^{(2)}\varepsilon)$ is taken as the second perturbation parameter relating to the dimensionless maximum deflection W_m, and $\lambda_T^{(i)}$ (i = 0, 2, 4…) are all functions of temperature, and the details of which may be found in Appendix C. The buckling temperatures as well as the thermal post-buckling load-deflection curves of auxetic GRMMC laminated cylindrical panels are then solved numerically. Note that an iterative numerical procedure is employed to obtain the solutions as the material properties of GRMMC panels are temperature-dependent (Shen and Xiang 2015).

4. Numerical investigations

This section presents the thermal post-buckling behaviors for GRMMC laminated cylindrical panels with in-plane NPR and resting on an elastic foundation. As cylindrical panels do not have the thermal bifurcation state, we will use flat panels for the comparison study to verify the current model and solution approach. The buckling temperatures $\alpha_0 T_{cr}$ for (0/90/0) and $(0/90)_S$ cross-ply laminated flat panel subjected to a uniform temperature rise are presented in Table 1 and are compared with the isogeometric FEM results of Tran *et al.* (2017) and Thanh *et al.* (2019). In Table 1, the panel has b/h = 10, a/b = 1 with material properties E_{11}/E_{22} = 15, G_{12}/E_{22} = G_{13}/E_{22} = 0.5, G_{23}/E_{22} = 0.3356, ν_{12} = 0.3, α_{11} = 0.015×10^{-6}/°C, α_{22}= 1.0 × 10^{-6}/°C, α_0 = 1.0 × 10^{-6}/°C. Good agreement is achieved between the current solutions and the results from Tran *et al.* (2017) and Thanh *et al.* (2019). The results reveal that the buckling temperature for the panel with fewer layers (for example, N = 3) is lower than that of the same panel with more layers (for example, N = 4).

The buckling temperatures T_{cr} are obtained for CNTRC flat panels subjected to a uniform temperature rise. Table 2 presents the current results and the Ritz method results of Mirzaei and Kiani (2016), the DQM results of Ansari *et al.* (2019) and the Galerkin method results of Tung and Trang (2020). The material properties come from Shen and Xiang (2015) and the panel has a/b = 1, h = 2 mm, b/h = 10 and 20. Good agreement between the current results and the results from Mirzaei and Kiani (2016), Ansari *et al.* (2019) and Tung and Trang (2020) is observed again.

Table 1 Comparison of buckling temperature $\alpha_0 T_{cr}$ for symmetric cross-ply laminated flat panels subjected to a uniform temperature rise, (m, n) = (1, 1)

Lay-up	Source	$\alpha_0 T_{cr}$
$(0/90)_S$	Present	0.0766
	Thanh *et al.* (2019)	0.0766
	Tran *et al.* (2017)	0.0762
(0/90/0)	Present	0.0754
	Thanh *et al.* (2019)	0.0754
	Tran *et al.* (2017)	0.0754

Table 2 Comparisons of buckling temperature T_{cr} (in K) for temperature dependent CNT/PMMA flat panels subjected to a uniform temperature rise [V_{CN}^* = 0.17, (m, n) = (1, 1)

b/h	Source	UD	FG-X
10	Present	399.44	419.09
	Mirzaei and Kiani (2016)	399.03	419.13
	Ansari *et al.* (2019)	398.94	419.10
	Tung and Trang (2020)	399.01	419.50
20	Present	343.00	359.52
	Mirzaei and Kiani (2016)	343.00	359.43
	Ansari *et al.* (2019)	342.98	359.46
	Tung and Trang (2020)	342.96	359.75

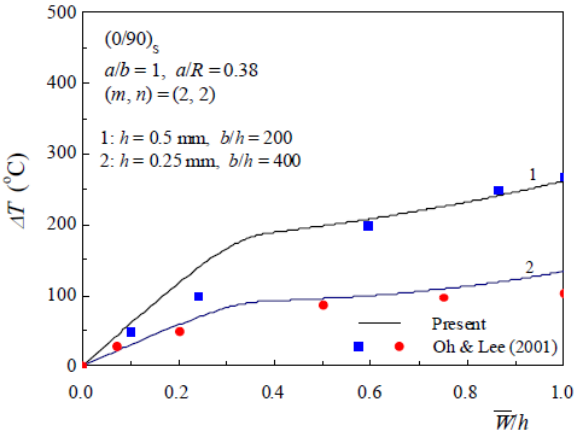

Fig. 2 Comparisons of thermal post-buckling load-deflection curves for $(0/90)_S$ laminated cylindrical panels subjected to a uniform temperature rise

Fig. 2 presents the thermal post-buckling results of a $(0/90)_S$ cross-ply laminated cylindrical panel from the current method and from the layerwise finite element results of Oh and Lee (2001). The panel is subjected to a uniform temperature rise and has a/R = 0.38, a/b = 1, b/h = 200 and 400. The material properties are: E_{11} = 138 GPa, E_{22} = 8.28 GPa, G_{12} = G_{13} = G_{23} = 6.9 GPa, ν_{12} = 0.33, α_{11} = 0.18×10^{-6}/°C, α_{22} = 27×10^{-6}/ °C. The present solution is in good agreement with that from Oh and Lee (2001). These results confirm that the thermal post-buckling load-deflection curve of the cylindrical panel is not the bifurcation type.

The comparison studies have validated the current

model and solution approach for the thermal post-buckling analysis of cylindrical panels. We then perform numerical investigations on the thermal post-buckling of auxetic GRMMC cylindrical panels. The panel is subjected to a uniform temperature rise and is rested on a Pasternak type

Table 3 Temperature-dependent coefficients for graphene/Cu composites

V_G	Properties	P_0	P_1	P_2	P_3
0.05	E_{11} (GPa)	241.8875	-0.15344	1.56964e-4	-9.00595e-8
	E_{22} (GPa)	221.4575	-0.10086	7.50357e-5	-4.67738e-8
	G_{12} (GPa)	74.37475	-0.03051	1.45893e-5	-5.40119e-9
	G_{13} (GPa)	35.66925	-0.00459	-7.74643e-6	7.72619e-10
	G_{23} (GPa)	28.99825	0.02529	-5.44964e-5	2.39006e-8
	ν_{12}	-0.00615	-3.48983e-4	6.25e-7	-3.81667e-10
	α_{11} (10^{-6}/K)	1.5377	-0.0011	2.85786e-6	-1.59524e-9
	α_{22} (10^{-6}/K)	1.5556	-0.00122	3.02857e-6	-1.63571e-9
0.07	E_{11} (GPa)	261.9775	-0.01568	-1.0075e-4	5.24167e-8
	E_{22} (GPa)	260.37	-0.09389	4.97857e-5	-3.75238e-8
	G_{12} (GPa)	81.392	0.00524	-3.45286e-5	1.32524e-8
	G_{13} (GPa)	24.3555	0.02055	-4.83643e-5	2.64595e-8
	G_{23} (GPa)	22.124	0.0348	-7.52e-5	4.06667e-8
	ν_{12}	0.00205	-3.23355e-4	4.60714e-7	-2.1881e-10
	α_{11} (10^{-6}/K)	-0.5509	0.00879	-1.31529e-5	6.63524e-9
	α_{22} (10^{-6}/K)	-0.65788	0.00939	-1.40868e-5	7.04536e-9
0.09	E_{11} (GPa)	300.8075	-0.085	1.07143e-7	4.5119e-9
	E_{22} (GPa)	279.785	-0.0955	7.84286e-5	-6.34524e-8
	G_{12} (GPa)	93.8735	0.00677	-5.625e-5	3.205e-8
	G_{13} (GPa)	30.5285	-0.02572	3.55929e-5	-1.84786e-8
	G_{23} (GPa)	26.897	-0.00733	3.02857e-6	-7.52381e-10
	ν_{12}	0.02263	-4.35363e-4	8.03214e-7	-4.77976e-10
	α_{11} (10^{-6}/K)	-0.62878	0.00861	-1.24054e-5	5.95107e-9
	α_{22} (10^{-6}/K)	-0.54615	0.00822	-1.19471e-5	5.8131e-9
0.11	E_{11} (GPa)	287.5875	0.1803	-4.55393e-4	2.35845e-7
	E_{22} (GPa)	303.5125	-0.05784	2.81071e-5	-6.36548e-8
	G_{12} (GPa)	134.8655	-0.12887	1.56364e-4	-6.88262e-8
	G_{13} (GPa)	8.20125	0.10503	-2.13889e-4	1.16868e-7
	G_{23} (GPa)	10.146	0.0893	-1.88571e-4	1.05048e-7
	ν_{12}	0.03558	-3.68413e-4	4.98214e-7	-2.32976e-10
	α_{11} (10^{-6}/K)	-1.44113	0.01213	-1.78539e-5	8.46512e-9
	α_{22} (10^{-6}/K)	-1.2885	0.01125	-1.63993e-5	7.73619e-9
0.13	E_{11} (GPa)	411.285	-0.46756	6.40929e-4	-3.30786e-7
	E_{22} (GPa)	372.9775	-0.36793	5.79321e-4	-3.60964e-7
	G_{12} (GPa)	165.8365	-0.2487	3.83879e-4	-2.01336e-7
	G_{13} (GPa)	18.66	0.0114	-2.72857e-5	1.39571e-8
	G_{23} (GPa)	28.83825	-0.05026	7.42107e-5	-3.67988e-8
	ν_{12}	0.15508	-0.00116	2.0575e-6	-1.09917e-9
	α_{11} (10^{-6}/K)	0.02517	0.00377	-4.63893e-6	2.16512e-9
	α_{22} (10^{-6}/K)	0.0368	0.0037	-4.42143e-6	1.99762e-9

Table 4 Effective Poisson's ratio ν_{12}^{e} for GRMMC laminates without deflection

T(K)	UD	FG-V	FG-Λ	FG-X	FG-O
			$(0/90/0/90/0)_S$		
300	-0.0472	-0.0496	-0.0496	-0.0449	-0.0449
500	-0.0527	-0.0600	-0.0600	-0.0564	-0.0564
700	-0.0513	-0.0585	-0.0585	-0.0528	-0.0528
1000	-0.0840	-0.0782	-0.0782	-0.0717	-0.0717
			$(0/90/0)_S$		
300	-0.0474	-0.0477	-0.0477	-0.0455	-0.0455
500	-0.0529	-0.0590	-0.0590	-0.0577	-0.0577
700	-0.0515	-0.0605	-0.0605	-0.0593	-0.0593
1000	-0.0845	-0.0750	-0.0750	-0.0750	-0.0750
			$(0/90)_{5T}$		
300	-0.0469	-0.0492	-0.0493	-0.0447	-0.0447
500	-0.0524	-0.0595	-0.0597	-0.0565	-0.0565
700	-0.0510	-0.0581	-0.0582	-0.0528	-0.0528
1000	-0.0831	-0.0772	-0.0777	-0.0717	-0.0717
			$(0/90)_{3T}$		
300	-0.0469	-0.0471	-0.0472	-0.0451	-0.0450
500	-0.0524	-0.0583	-0.0585	-0.0570	-0.0570
700	-0.0510	-0.0599	-0.0601	-0.0586	-0.0587
1000	-0.0831	-0.0736	-0.0740	-0.0728	-0.0728

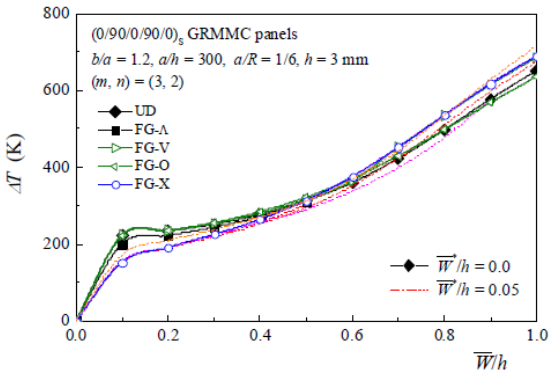

(a)

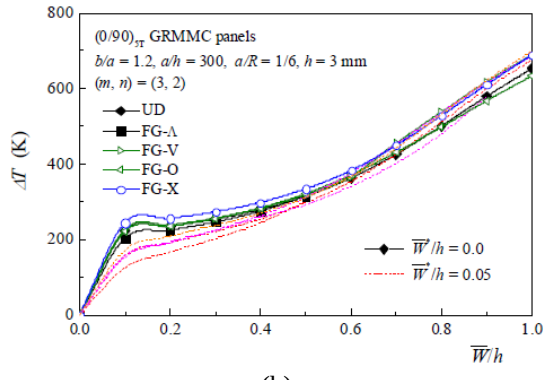

(b)

Fig. 3 Thermal post-buckling behavior of GRMMC cylindrical panels with in-plane NPR subjected to a uniform temperature rise: (a) $(0/90/0/90/0)_S$ panels; (b) $(0/90)_{5T}$ panels

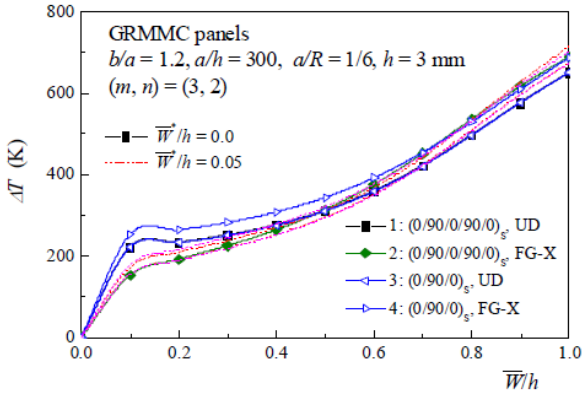

(a)

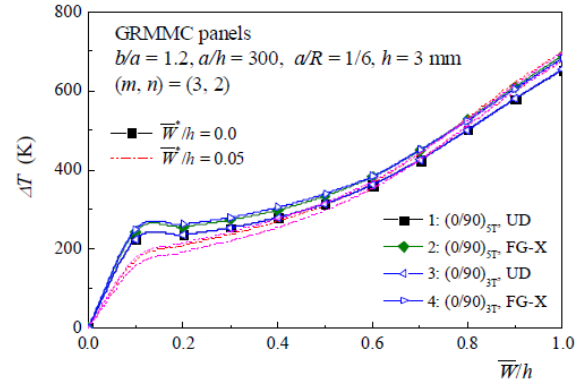

(b)

Fig. 4 Influence of total number of layers on the thermal post-buckling load-deflection curves of GRMMC cylindrical panels with in-plane NPR subjected to a uniform temperature rise: (a) $(0/90/0/90/0)_S$ and $(0/90/0/)_S$ panels; (b) $(0/90)_{5T}$ and $(0/90)_{3T}$ panels

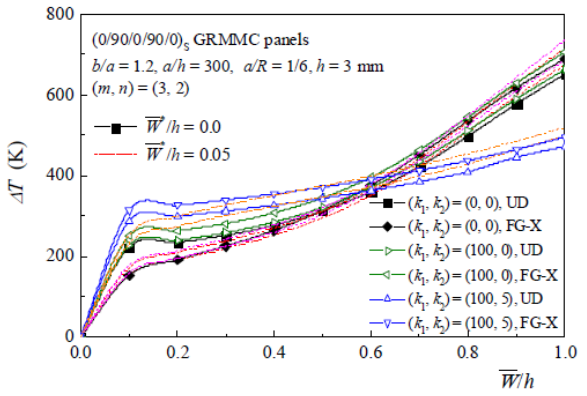

(a)

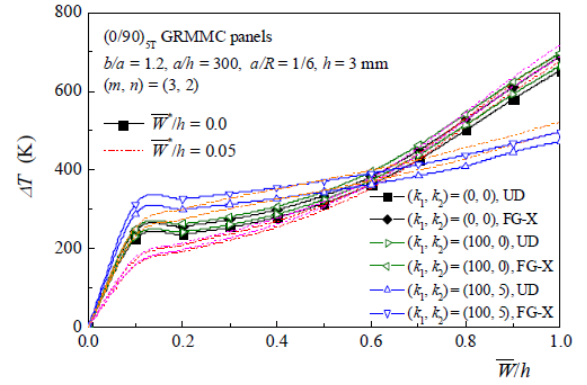

(b)

Fig. 5 Influence of foundation stiffness on the thermal post-buckling load-deflection curves of GRMMC cylindrical panels with in-plane NPR subjected to a uniform temperature rise: (a) $(0/90/0/90/0)_S$ panels; (b) $(0/90)_{5T}$ panels

foundation. The GRMMC layer is composed of copper matrix and graphene reinforcements (zigzag pattern refer to as 0-ply). Table 3 lists the effective material properties of the GRMMC layer of different graphene volume fractions (V_G = 0.05, 0.07, 0.09, 0.11 and 0.13). In the following, the panel geometric parameters are b/a = 1.2, a/h = 300 and a/R = 1/6. The layers have the same thickness and the panel thickness is h = 3 mm. 10-layer $(0/90/0/90/0)_S$ and $(0/90)_{5T}$ GRMMC laminated cylindrical panels are under consideration. The boundary condition is SSSS, except for the case in Fig. 6. The effective Poisson's ratio ν_{12}^e of the GRMMC laminated cylindrical panels can be determined once the FG pattern, the stack sequence and the orientation angles are chosen (Shen *et al.* 2020c, Shen and Xiang 2020). The effective Poisson's ratios ν_{12}^e for two GRMMC laminates in four different thermal environments T = 300 K, 500 K, 700 K and 1000 K are presented in Table 4.

Fig. 3 presents the thermal post-buckling responses for FG-Λ, FG-V, FG-O and FG-X $(0/90/0/90/0)_S$ and $(0/90)_{5T}$ panels subjected to a uniform temperature rise. The results for UD $(0/90/0/90/0)_S$ and $(0/90)_{5T}$ panels are also presented in Fig. 3. It has been reported that the panel has the bifurcation post-buckling path when movable in-plane condition is imposed to the two straight edges, whereas for the immovable in-plane condition case, the panel exhibits a limit-point post-buckling path (Shen and Xiang 2020). In the present example, the immovable in-plane conditions are considered and the thermal post-buckling equilibrium path of the panel is not the bifurcation-type. We observe that the FG-X $(0/90/0/90/0)_S$ panel has the lowest thermal post-buckling load-deflection curve, while the FG-X $(0/90)_{5T}$ panel has the highest thermal post-buckling load-deflection curve among the five cases when $\bar{W}/h$ < 0.6. The different behaviors of these two FG-X panels are due to the existence of the initial deflection caused by thermal bending in the FG-X $(0/90)_{5T}$ unsymmetric laminated panel while this initial deflection is absent in the FG-X $(0/90/0/90/0)_S$ symmetric laminated panel. It is noted that, in Fig. 3 and what follows, $\bar{W}^*/h$ is the dimensionless initial geometric imperfection, $\bar{W}/h$ is the dimensionless additional deflection, and (m, n) is the buckling mode where m and n represent the number of half waves in the X and Y directions, respectively.

Fig. 4 shows the relationship between the stacking sequence and the thermal post-buckling responses for UD and FG-X GRMMC laminated panels subjected to a uniform temperature rise. In Fig. 4, 6-layer $(0/90)_{3T}$ and $(0/90/0)_S$ panels are also considered and the FG-X patterns of the panels consist of $[0.13/0.09/0.05]_S$ layers. We observe that the effect of the number of layers on the

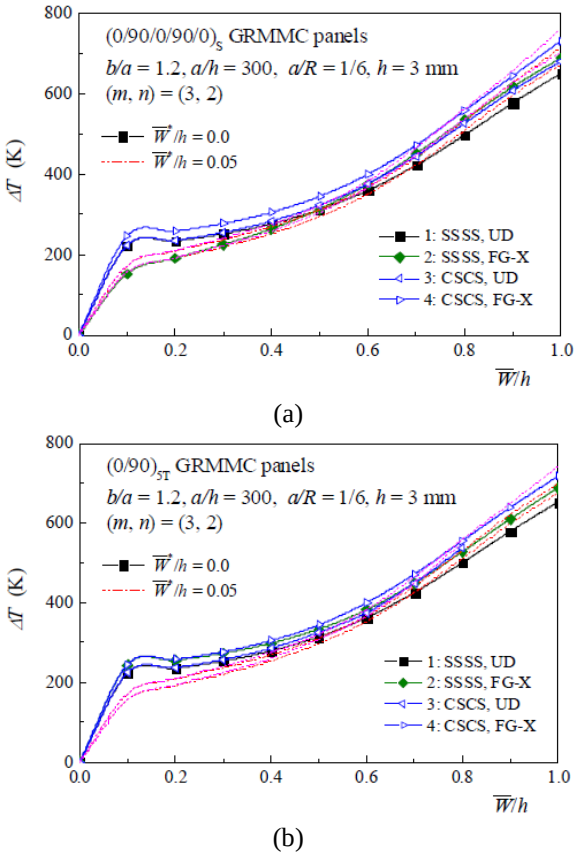

Fig. 6 Effect of boundary condition on the thermal post-buckling load-deflection curves of GRMMC cylindrical panels with in-plane NPR subjected to a uniform temperature rise: (a) $(0/90/0/90/0)_S$ panels; (b) $(0/90)_{5T}$ panels

thermal post-buckling load-deflection curves of UD GRMMC laminated panels is insignificant. Unlike the conventional observation, for the FG-X GRMMC panels, the 10-layer panel has a lower thermal post-buckling load-deflection curve than the 6-layer panel, in particular for the case of $(0/90/0)_S$ and $(0/90/0/90/0)_S$ GRMMC laminated cylindrical panels, which may be attributed to the influence of the in-plane NPR.

Fig. 5 depicts the impact of the foundation stiffness on the thermal post-buckling responses of UD and FG-X $(0/90/0/90/0)_S$ and $(0/90)_{5T}$ panels subjected to a uniform temperature rise. The panels rest on either the Winkler foundation with (k_1, k_2) = (100, 0) or the Pasternak foundation with (k_1, k_2) = (100, 5). As commonly shown, the thermal post-buckling load-deflection curves of panels increase when the foundation stiffness increases. Unlike in the compressive post-buckling case (Shen and Xiang 2020) where the post-buckling load-deflection curve is increased as foundation stiffness increases, in the present example, the panel exhibits a softer thermal post-buckling load-deflection curve with the Pasternak elastic foundation support than with the Winkler foundation or no foundation support when the panel deflection is sufficiently large.

Fig. 6 shows thermal post-buckling load-deflection curves for UD and FG-X $(0/90/0/90/0)_S$ and $(0/90)_{5T}$ panels subjected to a uniform temperature rise under two different boundary conditions. It is observed that the CSCS panels have higher thermal post-buckling load-deflection curves than their SSSS counterparts due to the two clamped edges provide stronger constraint than the two simply supported edges.

5. Conclusions

In the present paper, we examine the thermal post-buckling behaviors of FG-GRMMC laminated cylindrical panels with in-plane NPR. The panels are subjected to a uniform temperature rise and rest on an elastic foundation. The physical and mathematical models for the GRMMC laminated cylindrical panels under thermal loading conditions have been proposed. The novelty of this study is that it is the first study on the thermal post-buckling of GRMMC laminated cylindrical panels, considering the effect of the functionally graded configurations and the in-plane NPR. The temperature-dependent material properties of GRMMCs are estimated to obey a nonlinear function of temperature according to the MD simulation results. The results of numerical investigations show that the thermal post-buckling strength of $(0/90)_{5T}$ auxetic GRMMC panels can be enhanced as a result of the FG-X graphene reinforcement pattern. The main new finding is that due to the effect of in-plane NPR, the thermal post-buckling load-deflection curves of 6-layer $(0/90/0)_S$ and $(0/90)_{3T}$ GRMMC panels of FG-X pattern are higher than those of 10-layer $(0/90/0/90/0)_S$ and $(0/90)_{5T}$ GRMMC panels of FG-X pattern.

Conflict of interest

The authors declare that there are no conflicts of interests with publication of this work.

Acknowledgments

The supports for this work, provided by the National Natural Science Foundation of China (NSFC) under Grant 51779138, are gratefully acknowledged.

References

Alderson, K.L. and Coenen, V.L. (2008), "The low velocity impact response of auxetic carbon fibre laminates", *Phys. Stat. Sol. B*, **245**, 489-496. https://doi.org/10.1002/pssb.200777701.

Ansari, R., Torabi, J. and Hassani, R. (2019), "Thermal buckling analysis of temperature-dependent FG-CNTRC quadrilateral plates", *Comput. Math. Appl.*, **77**, 1294-1311. https://doi.org/10.1016/j.camwa.2018.11.009

Azoti, W.L., Koutsawa, Y., Bonfoh, N., Lipinski, P. and Belouettar, S. (2013), "Analytical modeling of multilayered dynamic sandwich composites embedded with auxetic layers", *Eng. Struct.*, **57**, 248-253. https://doi.org/10.1016/j.engstruct.2013.09.030.

Babaei, H., Kiani, Y. and Eslami, M.R. (2018), "Application of two-steps perturbation technique to geometrically nonlinear analysis of long FGM cylindrical panels on elastic foundation under thermal load", *J. Thermal Stress.*, **41**, 847-865. https://doi.org/ 10.1080/01495739.2017.1421054.

Babaei, H., Kiani, Y. and Eslami, M.R. (2019), "Large amplitude free vibrations of long FGM cylindrical panels on nonlinear elastic foundation based on physical neutral surface", *Compos. Struct.*, **220**, 888-898. https://doi.org/10.1016/j.compstruct.2019.03.064.

Bayat, M.R. and Mashhadi, M.M. (2018), "Low-velocity impact response of sandwich cylindrical panels with nanotube-reinforced and metal face sheet in thermal environment", *Aeronaut. J.*, **122**, 1943-1966. https://doi.org/10.1017/aer.2018.104.

Chen, X. and Feng, Z. (2017), "Dynamic behaviour of a thin laminated plate embedded with auxetic layers subject to in-plane excitation", *Mech. Res. Commun.*, **85**, 45-52. https://doi.org/ 10.1016/j.mechrescom.2017.07.013.

Clarke, J.F., Duckett, R.A., Hine, P.J., Hutchinson, I.J. and Ward, I.M. (1994), "Negative Poisson's ratios in angle-ply laminates: theory and experiment", *Compos.*, **25**, 863-868. https://doi.org/10.1016/0010-4361(94)90027-2.

Cong, P.H., Khanh, N.D., Khoa, N.D. and Duc, N.D. (2018), "New approach to investigate nonlinear dynamic response of sandwich auxetic double curves shallow shells using TSDT", *Compos. Struct.*, **185**, 455-465. https://doi.org/10.1016/j.compstruct.2017.11.047.

Dadkhah, M., Saboori, A. and Fino, P. (2019), "An overview of the recent developments in metal matrix nanocomposites reinforced by graphene", *Materials*, **12**, 2823. https://doi.org/10.3390/ma12172823.

Dehrouyeh-Semnani, A.M. and Jafarpour, S. (2019), "Nonlinear thermal stability of temperature-dependent metal matrix composite shallow arches with functionally graded fiber reinforcements", *Int. J. Mech. Sci.*, **161**, 105075. https://doi.org/10.1016/ j.ijmecsci.2019.105075.

Duc, N.D., Kim, S.-E., Tuan, N.D., Tran, P. and Khoa, N.D. (2017), "New approach to study nonlinear dynamic response and vibration of sandwich composite cylindrical panels with auxetic honeycomb core layer", *Aero. Sci. Tech.*, **70**, 396-404. https://doi.org/10.1016/j.ast.2017.08.023.

Duc, N.D. and Cong, P.H. (2018), "Nonlinear dynamic response and vibration of sandwich composite plates with negative Poisson's ratio in auxetic honeycombs", *J. Sandw. Struct. Mater.*, **20**, 692-717. https://doi.org/10.1177/1099636216674729.

Ebrahimi, F., Nouraei, M., Dabbagh, A. and Rabczuk, T. (2019), "Thermal buckling analysis of embedded graphene-oxide powder-reinforced nanocomposite plates", *Adv. Nano Res., Int. J.*, **7**(5), 293-310. https://doi.org/10.12989/anr.2019.7.5.293.

Evans, K.E., Donoghue, J.P. and Alderson, K.L. (2004), "The design, matching and manufacture of auxetic carbon fibre laminates", *J. Compos. Mater.*, **38**, 95-105. https://doi.org/ 10.1177/0021998304038645.

Fan, Y. and Wang, Y. (2021), "The effect of negative Poisson's ratio on the low-velocity impact response of an auxetic nanocomposite laminate beam", *Int. J. Mech. Mater. Des.*, **17**(1), 153-169. https://doi.org/ 10.1007/s10999-020-09521-x.

Fan, Y., Xiang, Y. and Shen, H.-S. (2019), "Temperature-dependent negative Poisson's ratio of monolayer graphene: Prediction from molecular dynamics simulations", *Nanotechnol. Rev.*, **8**, 415-421. https://doi.org/10.1515/ntrev-2019-0037.

Fan, Y., Xiang, Y. and Shen, H.-S. (2020), "Temperature-dependent mechanical properties of graphene/Cu nanocomposites with in-plane negative Poisson's ratios", *Research*, **2020**, 5618021. https://doi.org/10.34133/2020/5618021l.

Fattahi, A.M. and Sahmani, S. (2017), "Size dependency in the axial postbuckling behavior of nanopanels made of functionally graded material considering surface elasticity", *Arab. J. Sci. Eng.*, **42**, 4617-4633. https://doi.org/10.1007/s13369-017-2600-5.

Feldman, E. (1996), "The effect of temperature-dependent material properties on elasto-viscoplastic buckling behaviour of non-uniformly heated MMC plates", *Compos. Struct.*, **35**, 65-74. https://doi.org/10.1016/0263-8223(96)00024-4.

Feldman, E. and Aboudi, J. (1995), "Thermal postbuckling of metal matrix laminated plates", *J. Thermal Stress.*, **18**, 197-218. https://doi.org/10.1080/01495739508946299.

Harkati, E.H., Bezazi, A., Scarpa, F., Alderson, K. and Alderson, A. (2007), "Modelling the influence of the orientation and fibre reinforcement on the Negative Poisson's ratio in composite laminates", *Phys. Status Solidi B*, **244**, 883-892. https://doi.org/10.1002/ pssb.200572707.

Herakovich, C.T. (1984), "Composite laminates with Negative through-the-thickness Poisson's ratios", *J. Compos. Mater.*, **18**, 447-455. https://doi.org/10.1177/ 002199838401800504.

Hine, P.J., Duckett, R.A. and Ward, I.M. (1997), "Negative Poisson's ratios in angle-ply laminates", *J. Mater. Sci. Lett.*, **16**, 541-544. https://doi.org/10.1023/A:1018505503088.

Hu, Z., Tong, G., Lin, D., Chen, C., Guo, H., Xu, J. and Zhou, L. (2016), "Graphene-reinforced metal matrix nanocomposites-A review", *Mater. Sci. Technol.*, **32**, 930-953. https://doi.org/10.1080/02670836.2015.1104018.

Huang, C. and Chen, L. (2016), "Negative Poisson's ratio in modern functional materials", *Adv. Mater.*, **28**, 8079-8096. https://doi.org/10.1002/adma.201601363.

Huang, X.-H., Yang, J., Bai, L., Wang, X. and Ren, X. (2020a), "Theoretical solutions for auxetic laminated beam subjected to a sudden load", *Structures*, **28**, 57-68. https://doi.org/10.1016/j.istruc.2020.08.030.

Huang, X.-H., Yang, J., Wang, X. and Azim, I. (2020b), "Combined analytical and numerical approach for auxetic FG-CNTRC plate subjected to a sudden load", *Eng. with Comput.* https://doi.org/10.1007/s00366-020-01106-8.

Karami, B. and Karami, S. (2019), "Buckling analysis of nanoplate-type temperature-dependent heterogeneous materials", *Adv. Nano Res., Int. J.*, **7**(1), 51-61. https://doi.org/10.12989/ anr.2019.7.1.051.

Kiani, Y. (2018), "NURBS-based isogeometric thermal postbuckling analysis of temperature dependent graphene reinforced composite laminated plates", *Thin-Walled Struct.*, **125**, 211-219. https://doi.org/10.1016/j.tws.2018.01.024.

Kiani, Y. and Mirzaei, M. (2018), "Enhancement of non-linear thermal stability of temperature dependent laminated beams with graphene reinforcements", *Compos. Struct.*, **186**, 114-122. https://doi.org/10.1016/j.compstruct.2017.11.086.

Lakes, R.S. (2017), "Negative-Poisson's-ratio materials: Auxetic solids", *Annu. Rev. Mater. Res.*, **47**, 63-81. https://doi.org/10.1146/annurev-matsci-070616-124118.

Lal, A., Singh, B.N. and Kale, S., (2012), "Stochastic thermal post-buckling response of laminated composite cylindrical shell panel with system randomness", *Int. J. Appl. Mech.*, **4**, 1250009. https://doi.org/10.1142/S1758825112001385.

Lee, J.J., Oh, I.-K., Lee, I. and Yeom, C.H. (2002), "Thermal post-buckling behavior of patched laminated panels under uniform and non-uniform temperature distributions", *Compos. Struct.*, **55**, 137-145. https://doi.org/10.1016/S0263-8223(01)00139-8.

Li, C., Shen, H.-S. and Wang, H. (2019a), "Thermal post-buckling of sandwich beams with functionally graded negative Poisson's ratio honeycomb core", *Int. J. Mech. Sci.*, **152**, 289-297. https://doi.org/10.1016/j.ijmecsci.2019.01.002.

Li, C., Shen, H.-S. and Wang, H. (2019b), "Nonlinear bending of

sandwich beams with functionally graded negative Poisson's ratio honeycomb core", *Compos. Struct*., **212**, 317-325. https://doi.org/10.1016/j.compstruct.2019.01.020.

Li, C., Shen, H.-S. and Wang, H. (2019c), "Nonlinear dynamic response of sandwich beams with functionally graded negative Poisson's ratio honeycomb core", *Euro. Phys. J. Plus*, **134**, 79. https://doi.org/10.1140/epjp/i2019-12572-7.

Li, C., Shen, H.-S. and Wang, H. (2019d), "Nonlinear vibration of sandwich beams with functionally graded negative Poisson's ratio honeycomb core", *Int. J. Struct. Stabil. Dyn*., **19**, 1950034. https://doi.org/10.1142/S0219455419500342.

Li, C., Shen, H.-S. and Wang, H. (2020a), "Postbuckling behavior of sandwich plates with functionally graded auxetic 3D lattice core", *Compos. Struct*., **237**, 111894. https://doi.org/10.1016/j.compstruct.2020.111894.

Li, C., Shen, H.-S., Wang, H. and Yu, Z. (2020b), "Large amplitude vibration of sandwich plates with functionally graded auxetic 3D lattice core", *Int. J. Mech. Sci*., **174**, 105472. https://doi.org/10.1016/j.ijmecsci.2020.105472.

Li, C., Shen, H.-S. and Wang, H. (2020c), "Nonlinear dynamic response of sandwich plates with functionally graded auxetic 3D lattice core", *Nonlinear Dyn*., **100**, 3235-3252. https://doi.org/10.1007/s11071-020-05686-4.

Li, C., Shen, H.-S. and Wang, H. (2020d), "Full-scale finite element modeling and nonlinear bending analysis of sandwich plates with functionally graded auxetic 3D lattice core", *J. Sandw. Struct. Mater*. https://doi.org/10.1177/1099636220924657.

Liang, Q., Yao, X., Wang, W., Liu, Y. and Wong, C.P. (2011), "A three-dimensional vertically aligned functionalized multilayer graphene architecture: an approach for graphene-based thermal interfacial materials", *ACS Nano*, **5**, 2392-2401. https://doi.org/10.1021/nn200181e.

Lin, F., Xiang, Y. and Shen, H.-S. (2017), "Temperature dependent mechanical properties of graphene reinforced polymer nanocomposites - a molecular dynamics simulation", *Compos. Part B-Eng*., **111**, 261-269. https://doi.org/10.1016/j.compositesb.2016.12.004.

Liu, Q. (2006), "Literature review: Materials with negative Poisson's ratios and potential applications to aerospace and defence", Report no. dsto-gd-0472, Defence Science and Technology Organisation, Department of Defence, Australian Government.

Ma, W., Yang, C., Ma, D. and Zhong, J.L. (2019), "Low-velocity impact response of nanotube-reinforced composite sandwich curved panels", *SADHANA-Academy Proc. Eng. Sci*., **44**, 227. https://doi.org/10.1007/s12046-019-1214-x.

Mehar, K. and Panda, S.K. (2019), "Multiscale modeling approach for thermal buckling analysis of nanocomposite curved structure", *Adv. Nano Res., Int. J*., **7**(3), 181-190. https://doi.org/10.12989/anr.2019.7.3.179.

Milton, G.W. (1992), "Composite materials with Poisson's ratios close to - 1", *J. Mech. Phys. Solids*., **40**, 1105-1137. https://doi.org/10.1016/0022-5096(92)90063-8.

Mir, M., Ali, M.N., Sami, J. and Ansari, U. (2014), "Review of mechanics and applications of auxetic structures", *Adv. Mater. Sci. Eng*., 2014, 753496. https://doi.org/10.1155/2014/753496.

Mirzaei, M. and Kiani, Y. (2016), "Thermal buckling of temperature dependent FG-CNT reinforced composite plates", *Meccanica*, **51**, 2185-2201. https://doi.org/10.1007/s11012-015-0348-0.

Mirzaei, M. and Kiani, Y. (2017), "Isogeometric thermal buckling analysis of temperature dependent FG graphene reinforced laminated plates using NURBS formulation", *Compos. Struct*., **180**, 606-616. https://doi.org/10.1016/j.compstruct.2017.08.057.

Naseer, A., Ahmad, F., Aslam, M., Guan, B.H., Wan Harund, W.S., Muhamade, N., Razaf, M.R. and German, R.M. (2019), "A review of processing techniques for graphene-reinforced metal matrix composites", *Mater. Manufact. Process*., **34**, 957-985. https://doi.org/ 10.1080/10426914.2019.1615080.

Ni, Z., Bu, H., Zou, M., Yi, H., Bi, K. and Chen, Y. (2010), "Anisotropic mechanical properties of graphene sheets from molecular dynamics", *Physica B*, **405**, 1301-1306. https://doi.org/ 10.1016/j.physb.2009.11.071.

Novoselov, K.S., Geim, A.K., Morozov, S.V., Jiang, D., Zhang, Y., Dubonos, S.V., Grigorieva, I.V. and Firsov, A. (2004), "Electric filed effect in atomically thin carbon films", *Science*, **306**, 666-669. https://doi.org/10.1126/science.1102896.

Oh, I.K. and Lee, I. (2001), "Thermal snapping and vibration characteristics of cylindrical composite panels using layerwise theory", *Compos. Struct*., **51**, 49-61. https://doi.org/10.1016/S0263-8223(00)00123-9.

Panda, S.K. and Singh, B.N. (2009), "Thermal post-buckling behaviour of laminated composite cylindrical/hyperboloid shallow shell panel using nonlinear finite element method", *Compos. Struct*., **91**, 366-374. https://doi.org/10.1016/j.compstruct.2009.06.004.

Panda, S.K. and Singh, B.N. (2013), "Post-buckling analysis of laminated composite doubly curved panel embedded with SMA fibers subjected to thermal environment", *Mech. Adv. Mater. Struct*., **20**, 842-853. https://doi.org/10.1080/15376494.2012.677097.

Paley, M. and Aboudi, J. (1991), "Inelastic thermal buckling of metal matrix laminated plates", *J. Thermal Stress*., **14**, 479-497. https://doi.org/10.1080/01495739108927081.

Prawoto, Y. (2012), "Seeing auxetic materials from the mechanics point of view: A structural review on the negative Poisson's ratio", *Comput. Mater. Sci*., **58**, 140-153. https://doi.org/ 10.1016/j.commatsci.2012.02.012.

Reddy, J.N. and Liu, C.F. (1985), "A higher-order shear deformation theory of laminated elastic shells", *Int. J. Eng. Sci*., **23**, 319-330. https://doi.org/10.1016/0020-7225(85)90051-5.

Ren, X., Das, R., Tran, P., Ngo, T.D. and Xie, Y.M. (2018), "Auxetic metamaterials and structures: a review", *Smart Mater. Struct*., **27**, 023001. https://doi.org/10.1088/1361-665X/aaa61c.

Roh, J.H., Oh, I.K., Yang, S.M., Han, J.H. and Lee, I. (2004), "Thermal post-buckling analysis of shape memory alloy hybrid composite shell panels", *Smart Mater. Struct*., **13**, 1337-1344. https://doi.org/10.1088/0964-1726/13/6/006.

Sahmani, S. and Fattahi, A.M. (2017), "Imperfection sensitivity of the size-dependent nonlinear instability of axially loaded FGM nanopanels in thermal environments", *Acta Mech*., **228**, 3789-3810. https://doi.org/10.1007/s00707-017-1912-6.

Saxena, K.K., Das, R. and Calius, E.P. (2016), "Three decades of auxetics research-materials with negative Poisson's ratio: A review", *Adv. Eng. Mater*., **18**, 1847-1870. https://doi.org/10.1002/adem.201600053

Sharma, S., Kumar, P. and Chandra, R. (2017), "Mechanical and thermal properties of graphene-carbon nanotube-reinforced metal matrix composites: A molecular dynamics study", *J. Compos. Mater*., **51**, 3299-3313. https://doi.org/10.1177/0021998316682363.

She, G.L., Yuan, F.G. and Ren, Y.R. (2017), "Research on nonlinear bending behaviors of FGM infinite cylindrical shallow shells resting on elastic foundations in thermal environments", *Compos. Struct*., **170**, 111-121. https://doi.org/10.1016/j.compstruct.2017.03.010.

Shen, H.-S. (2009a), *Functionally Graded Materials Nonlinear Analysis of Plates and Shells*, CRC Press, Boca Raton.

Shen, H.-S. (2009b), "Nonlinear bending of functionally graded carbon nanotube-reinforced composite plates in thermal environments", *Compos, Struct*., **91**, 9-19. https://doi.org/10.1016/ j.compstruct.2009.04.026.

Shen, H.-S. (2013), *A Two-Step Perturbation Method in Nonlinear*

Analysis of Beams, Plates and Shells, John Wiley & Sons Inc.

Shen, H.-S. (2017), *Postbuckling Behavior of Plates and Shells*, World Scientific Publishing Co. Pte. Ltd., Singapore.

Shen, H.-S. and Wang, H. (2013), "Thermal postbuckling of functionally graded fiber reinforced composite cylindrical shells surrounded by an elastic medium", *Compos. Struct*., **102**, 250-260. https://doi.org/10.1016/j.compstruct.2013.03.011.

Shen, H.-S. and Xiang, Y. (2015), "Thermal postbuckling of nanotube-reinforced composite cylindrical panels resting on elastic foundations", *Compos. Struct*., **123**, 383-392. https://doi.org/ 10.1016/j.compstruct.2014.12.059.

Shen, H.-S., and Xiang, Y. (2019), "Thermal buckling and postbuckling behavior of FG-GRC laminated cylindrical shells with temperature-dependent material properties", *Meccanica*, **54**, 283-297. https://doi.org/10.1007/s11012-019-00945-0.

Shen, H.-S. and Xiang, Y. (2020), "Effect of negative Poisson's ratio on the axially compressed postbuckling behavior of FG-GRMMC laminated cylindrical panels on elastic foundations", *Thin-Walled Struct*., **157**, 107090. https://doi.org/10.1016/j.tws.2020.107090.

Shen, H.-S., Lin, F. and Xiang, Y. (2017a), "Nonlinear bending and thermal postbuckling of functionally graded graphene-reinforced composite laminated beams resting on elastic foundations", *Eng. Struct*., **140**, 89-97. https://doi.org/10.1016/j.engstruct.2017.02.069.

Shen, H.-S., Xiang, Y. and Lin, F. (2017b), "Thermal buckling and postbuckling of functionally graded graphene-reinforced composite laminated plates resting on elastic foundations", *Thin-Walled Struct*., **118**, 229-237. https://doi.org/10.1016/j.tws.2017.05.006.

Shen, H.-S., Xiang, Y. and Fan, Y. (2019a), "Large amplitude vibration of doubly curved FG-GRC laminated panels in thermal environments", *Nanotechnol. Rev*., **8**, 467-483. https://doi.org/ 10.1515/ntrev-2019-0042.

Shen, H.-S., Xiang, Y. and Reddy, J.N. (2019b), "Thermal postbuckling behavior of FG-GRC laminated cylindrical panels with temperature-dependent properties", *Compos. Struct*., **211**, 433-442. https://doi.org/10.1016/j.compstruct.2018.12.023.

Shen, H.-S., Li, C. and Reddy, J.N. (2020a), "Large amplitude vibration of FG-CNTRC laminated cylindrical shells with negative Poisson's ratio", *Comput. Methods Appl. Mech. Eng*., 360, 112727. https://doi.org/10.1016/j.cma.2019.112727.

Shen, H.-S., Huang, X.-H. and Yang, J. (2020b), "Nonlinear bending of temperature-dependent FG-CNTRC laminated plates with negative Poisson's ratio", *Mech. Adv. Mater. Struct*., **27**, 1141-1153. https://doi.org/10.1080/15376494.2020.1716412.

Shen, H.-S., Xiang, Y. and Reddy, J.N. (2020c), "Effect of negative Poisson's ratio on the post-buckling behavior of FG-GRMMC laminated plates in thermal environments", *Compos. Struct*., **253**, 112731. https://doi.org/10.1016/j.compstruct.2020.112731.

Shen, L., Shen, H.-S. and Zhang, C.L. (2010), "Temperature-dependent elastic properties of single layer graphene sheets", *Mater. Des*., **31**, 4445-4449. https://doi.org/10.1016/j.matdes.2010.04.016.

Sun, C.T. and Li, S.J. (1988), "Three-dimensional effective elastic constants for thick laminates", *J. Compos. Mater*., **22**, 629-639. https://doi.org/10.1177/002199838802200703.

Tabandeh-Khorshid, M., Kumar, A., Omrani, E., Kim, C. and Rohatgi, P. (2020), "Synthesis, characterization, and properties of graphene reinforced metal-matrix nanocomposites", *Compos. Part B-Eng*., **183**, 107664. https://doi.org/ 10.1016/j.compositesb.2019.107664.

Thanh, C.L., Tran, L.V., Vu-Huu, T. and Abdel-Wahab, M. (2019), "The size-dependent thermal bending and buckling analyses of composite laminate microplate based on new modified couple stress theory and isogeometric analysis", *Comput. Methods Appl. Mech. Eng*., **350**, 337-361. https://doi.org/10.1016/j.cma.2019.02.028.

Tran, L.V., Wahab, M.A. and Kim, S.E. (2017), "An isogeometric finite element approach for thermal bending and buckling analyses of laminated composite plates", *Compos. Struct*., **179**, 35-49. https://doi.org/10.1016/j.compstruct.2017.07.056.

Trang, L.T.N. and Tung, H.V. (2020), "Thermally induced postbuckling of higher order shear deformable CNT-reinforced composite flat and cylindrical panels resting on elastic foundations with elastically restrained edges", *Mech. Based Des. Struct. Machin*., 1-24. https://doi.org/10.1080/15397734.2020.1785312.

Tung, H.V. and Trang, L.T.N. (2020), "Thermal postbuckling of shear deformable CNT-reinforced composite plates with tangentially restrained edges and temperature-dependent properties", *J. Thermoplastic Compos. Mater*., **33**, 97-124. https://doi.org/10.1177/ 0892705718804588.

Yang, J., Huang, X.-H. and Shen, H.-S. (2020a), "Nonlinear vibration of temperature-dependent FG-CNTRC laminated plates with negative Poisson's ratio", *Thin-Walled Struct*., **148**, 106514. https://doi.org/10.1016/j.tws.2019.106514.

Yang, J., Huang, X.-H. and Shen, H.-S. (2020b), "Nonlinear flexural behavior of temperature-dependent FG-CNTRC laminated beams with negative Poisson's ratio resting on the Pasternak foundation", *Eng. Struct*., **207**, 110250. https://doi.org/10.1016/ j.engstruct.2020.110250.

Yang, J., Huang, X.-H. and Shen, H.-S. (2020c), "Nonlinear vibration of temperature-dependent FG-CNTRC laminated beams with negative Poisson's Ratio", *Int. J. Struct. Stabil. Dyn*., **20**, 2050043. https://doi.org/10.1142/S0219455420500431.

Yeh, H.L. amd Yeh, H.Y. (1999), "A discussion of negative poisson's ratio design for composites", *J. Reinf. Plastics Compos*., **18**, 1546-1556. https://doi.org/ 10.1177/073168449901801701.

Yu, Y. and Shen, H.-S. (2020a), "A comparison of nonlinear vibration and bending of hybrid CNTRC/metal laminated plates with positive and negative Poisson's ratios", *Int. J. Mech. Sci*., **183**, 105790. https://doi.org/10.1016/j.ijmecsci.2020.105790.

Yu, Y. and Shen, H.-S. (2020b), "A comparison of nonlinear bending and vibration of hybrid metal/CNTRC laminated beams with positive and negative Poisson's ratios", *Int. J. Struct. Stabil. Dyn*., **20**, 2043007. https://doi.org/10.1142/S021945542043007.5

Zhang, J., Zhu, X., Yang, X. and Zhang, W. (2019), "Transient nonlinear responses of an auxetic honeycomb sandwich plate under impact loads", *Int. J. Impact Eng*., **134**, 103383. https://doi.org/10.1016/j.ijimpeng.2019.103383.

Zhang, R., Yeh, H.L. and Yeh, H.Y. (1998), "A preliminary study of negative Poisson's ratio of laminated fiber reinforced composites", *J. Reinf. Plastics Compos*., **17**, 1651-1664. https://doi.org/10.1177/073168449801701806.

Zhao, Y.X., Liu, T. and Li, Z.M. (2018), "Nonlinear bending analysis of a 3D braided composite cylindrical panel subjected to transverse loads in thermal environments", *Chinese J. Aeron*., **31**, 1716-1727. https://doi.org/10.1016/j.cja.2018.03.022.

AT

Appendix A

In Eq. (2), the thermal internal forces $\bar{N}^T$, $\bar{M}^T$ and $\bar{S}^T$ can be calculated by

$$\begin{bmatrix} \bar{N}_x^T & \bar{M}_x^T & \bar{P}_x^T \\ \bar{N}_y^T & \bar{M}_y^T & \bar{P}_y^T \\ \bar{N}_{xy}^T & \bar{M}_{xy}^T & \bar{P}_{xy}^T \end{bmatrix} = \sum_{k=1}^{N} \int_{h_{k-1}}^{h_k} \begin{bmatrix} A_x \\ A_y \\ A_{xy} \end{bmatrix}_k (1, Z, Z^3) \Delta T dZ \tag{A.1a}$$

and $\bar{S}^T$ is given by

$$\begin{bmatrix} \bar{S}_x^T \\ \bar{S}_y^T \\ \bar{S}_{xy}^T \end{bmatrix} = \begin{bmatrix} \bar{M}_x^T \\ \bar{M}_y^T \\ \bar{M}_{xy}^T \end{bmatrix} - \frac{4}{3h^2} \begin{bmatrix} \bar{P}_x^T \\ \bar{P}_y^T \\ \bar{P}_{xy}^T \end{bmatrix} \tag{A.1b}$$

where $\Delta T = T - T_0$ is the temperature increment with regard to the reference temperature of T_0 (300 K) at which the panel has no initial thermal stresses, and

$$\begin{bmatrix} A_x \\ A_y \\ A_{xy} \end{bmatrix} = - \begin{bmatrix} \bar{Q}_{11} & \bar{Q}_{12} & \bar{Q}_{16} \\ \bar{Q}_{12} & \bar{Q}_{22} & \bar{Q}_{26} \\ \bar{Q}_{16} & \bar{Q}_{26} & \bar{Q}_{66} \end{bmatrix} \begin{bmatrix} c^2 & s^2 \\ s^2 & c^2 \\ 2cs & -2cs \end{bmatrix} \begin{bmatrix} \alpha_{11} \\ \alpha_{22} \end{bmatrix} \tag{A.2}$$

where α_{11} and α_{22} are the thermal expansion coefficients of the kth ply, and the terms $\bar{Q}_{ij}$ may be written as

$$\begin{bmatrix} \bar{Q}_{11} \\ \bar{Q}_{12} \\ \bar{Q}_{22} \\ \bar{Q}_{16} \\ \bar{Q}_{26} \\ \bar{Q}_{66} \end{bmatrix} = \begin{bmatrix} c^4 & 2c^2s^2 & s^4 & 4c^2s^2 \\ c^2s^2 & c^4+s^4 & c^2s^2 & -4c^2s^2 \\ s^4 & 2c^2s^2 & c^4 & 4c^2s^2 \\ c^3s & cs^3-c^3s & -cs^3 & -2cs(c^2-s^2) \\ cs^3 & c^3s-cs^3 & -c^3s & 2cs(c^2-s^2) \\ c^2s^2 & -2c^2s^2 & c^2s^2 & (c^2-s^2)^2 \end{bmatrix} \begin{bmatrix} Q_{11} \\ Q_{12} \\ Q_{22} \\ Q_{66} \end{bmatrix} \tag{A.3a}$$

$$\begin{bmatrix} \bar{Q}_{44} \\ \bar{Q}_{45} \\ \bar{Q}_{55} \end{bmatrix} = \begin{bmatrix} c^2 & s^2 \\ -cs & cs \\ s^2 & c^2 \end{bmatrix} \begin{bmatrix} Q_{44} \\ Q_{55} \end{bmatrix} \tag{A.3b}$$

where

$$\begin{bmatrix} Q_{11} \\ Q_{12} \\ Q_{22} \\ Q_{66} \end{bmatrix} = \begin{bmatrix} \frac{1}{1-v_{12}v_{21}} & 0 & 0 & 0 \\ 0 & \frac{v_{21}}{1-v_{12}v_{21}} & 0 & 0 \\ 0 & 0 & \frac{1}{1-v_{12}v_{21}} & 0 \\ 0 & 0 & 0 & 1 \end{bmatrix} \begin{bmatrix} E_{11} \\ E_{11} \\ E_{22} \\ G_{12} \end{bmatrix} \tag{A.4a}$$

$$Q_{44} = G_{23}, Q_{55} = G_{13} \tag{A.4b}$$

in which E_{11}, E_{22}, G_{12}, G_{13}, G_{23}, ν_{12} and ν_{21} have their usual meaning for the GRMMC layer.

Appendix B

The solutions of W, Ψ_x, Ψ_y and F for the GRMMC laminated cylindrical panel may be written as

$$\begin{aligned} W = \varepsilon & \left[A_{00}^{(1)} - A_{00}^{(1)} \left(a_{01}^{(1)} \cos\varphi \frac{x}{\sqrt{\varepsilon}} + a_{10}^{(1)} \sin\varphi \frac{x}{\sqrt{\varepsilon}} \right) \right. \\ & exp\left(-\vartheta \frac{x}{\sqrt{\varepsilon}}\right) - A_{00}^{(1)} \left(a_{01}^{(1)} \cos\varphi \frac{\pi - x}{\sqrt{\varepsilon}} + a_{10}^{(1)} \sin\varphi \frac{\pi - x}{\sqrt{\varepsilon}} \right) \\ & \left. exp\left(-\vartheta \frac{\pi - x}{\sqrt{\varepsilon}}\right) \right] + \varepsilon^2 - A_{02}^{(2)} (\cos 2ny - 1) \\ & \left(a_{01}^{(1)} \cos\varphi \frac{x}{\sqrt{\varepsilon}} + a_{10}^{(1)} \sin\varphi \frac{x}{\sqrt{\varepsilon}} \right) - A_{02}^{(2)} (\cos 2ny - 1) \\ & \left(a_{01}^{(1)} \cos\varphi \frac{\pi - x}{\sqrt{\varepsilon}} + a_{10}^{(1)} \sin\varphi \frac{\pi - x}{\sqrt{\varepsilon}} \right) exp\left(-\vartheta \frac{\pi - x}{\sqrt{\varepsilon}}\right) \Big] \\ & + \varepsilon^3 \left[A_{11}^{(3)} \sin mx \ \sin ny + A_{02}^{(3)} (\cos 2ny - 1) \right] \\ & + \varepsilon^4 \left[A_{00}^{(4)} + A_{11}^{(4)} \sin mx \ \sin ny + A_{20}^{(4)} \cos 2mx \right. \\ & + A_{02}^{(4)} (\cos 2ny - 1) + A_{13}^{(4)} \sin mx \ \sin 3ny \\ & \left. + A_{04}^{(4)} (\cos 4ny - 1) \right] + O(\varepsilon^5) \end{aligned} \tag{B.1}$$

$$\begin{aligned} \Psi_x = & \varepsilon^{\frac{3}{2}} \left[A_{00}^{(1)} c_{10}^{\left(\frac{3}{2}\right)} \sin\varphi \frac{x}{\sqrt{\varepsilon}} exp\left(-\vartheta \frac{x}{\sqrt{\varepsilon}}\right) \right. \\ & + A_{00}^{(1)} c_{10}^{\left(\frac{3}{2}\right)} \sin\varphi \frac{\pi - x}{\sqrt{\varepsilon}} + \varepsilon^2 \left[C_{11}^{(2)} \cos mx \ \sin ny \right] \\ & + \varepsilon^{\frac{5}{2}} \left[A_{02}^{(2)} (\cos 2ny - 1) c_{10}^{\left(\frac{5}{2}\right)} \sin\varphi \frac{x}{\sqrt{\varepsilon}} exp\left(-\vartheta \frac{x}{\sqrt{\varepsilon}}\right) \right. \\ & + A_{02}^{(2)} (\cos 2ny - 1) c_{10}^{\left(\frac{5}{2}\right)} \sin\varphi \frac{\pi - x}{\sqrt{\varepsilon}} \\ & \left. exp\left(-\vartheta \frac{\pi - x}{\sqrt{\varepsilon}}\right) \right] + \varepsilon^3 [C_{11}^{(3)} \cos mx \ \sin ny \\ & + \varepsilon^4 [C_{11}^{(4)} \cos mx \ \sin ny + C_{20}^{(4)} \sin 2mx \\ & + C_{13}^{(4)} \cos mx \ \sin 3ny] + O(\varepsilon^5) \end{aligned} \tag{B.2}$$

$$\begin{aligned} \Psi_y = & \varepsilon^2 \left[D_{11}^{(2)} \sin mx \ \cos ny \right] \\ & + \varepsilon^3 [D_{11}^{(3)} \sin mx \ \cos ny + D_{02}^{(3)} \sin 2ny \\ & + \varepsilon^4 [D_{11}^{(4)} \sin mx \ \cos ny + D_{02}^{(4)} \sin 2ny \\ & + D_{13}^{(4)} \sin mx \ \cos 3ny] + O(\varepsilon^5) \end{aligned} \tag{B.3}$$

$$\begin{aligned} F = & - B_{00}^{(0)} \frac{y^2}{2} + \varepsilon \left[-B_{00}^{(1)} \frac{y^2}{2} \right] \\ & + \varepsilon^2 \left[-B_{00}^{(2)} \frac{y^2}{2} + B_{11}^{(2)} \sin mx \ \sin ny \right. \\ & + A_{00}^{(1)} \left(b_{01}^{(2)} \cos\varphi \frac{x}{\sqrt{\varepsilon}} + b_{10}^{(2)} \sin\varphi \frac{x}{\sqrt{\varepsilon}} \right) exp\left(-\vartheta \frac{x}{\sqrt{\varepsilon}}\right) \\ & + A_{00}^{(1)} \left(b_{01}^{(2)} \cos\varphi \frac{\pi - x}{\sqrt{\varepsilon}} + b_{10}^{(2)} \sin\varphi \frac{\pi - x}{\sqrt{\varepsilon}} \right) \\ & exp\left(-\vartheta \frac{\pi - x}{\sqrt{\varepsilon}}\right) \Big] + \varepsilon^3 \left[-B_{00}^{(3)} \frac{y^2}{2} + B_{02}^{(3)} \cos 2ny \right. \\ & + A_{02}^{(2)} (\cos 2ny - 1) \left(b_{01}^{(3)} \cos\varphi \frac{x}{\sqrt{\varepsilon}} + b_{10}^{(3)} \sin\varphi \frac{x}{\sqrt{\varepsilon}} \right) \\ & exp\left(-\vartheta \frac{x}{\sqrt{\varepsilon}}\right) + A_{02}^{(2)} (\cos 2ny - 1) \\ & \left(b_{01}^{(3)} \cos\varphi \frac{\pi - x}{\sqrt{\varepsilon}} + b_{10}^{(3)} \sin\varphi \frac{\pi - x}{\sqrt{\varepsilon}} \right) \\ & exp\left(-\vartheta \frac{\pi - x}{\sqrt{\varepsilon}}\right) \Big] + \varepsilon^4 \left[-B_{00}^{(4)} \frac{y^2}{2} - b_{00}^{(4)} \frac{x^2}{2} \right. \\ & + B_{20}^{(4)} \cos 2mx + B_{02}^{(4)} \cos 2ny \\ & \left. - B_{13}^{(4)} \sin mx \ \sin 3ny \right] + O(\varepsilon^5) \end{aligned} \tag{B.4}$$

In Eq. (B.1), the term $A_{00}^{(1)}$ is expanded by Fourier sine series in the *y* direction as

$$\frac{4}{\pi}A_{00}^{(1)}\sum_{j=1,3,\ldots}\frac{1}{j}\sin j\,y \tag{B.5}$$

To this end, the boundary condition $w_1 = 0$ at $y = 0,\ \pi$ can be satisfied and $A_{00}^{(1)}$ remains a constant in the *x* direction. In Eqs. (B.1)-(B.4), all coefficients are related and can be expressed in terms of $A_{11}^{(2)}$, an

$$A_{11}^{(2)}\varepsilon = W_m - \Theta_2 W_m^2 + \cdots \tag{B.6}$$

where W_m is the dimensionless form of the maximum deflection of the panel and is given by

$$W_m = \frac{1}{C_{33}}\left[\frac{h}{[D_{11}^* D_{22}^* A_{11}^* A_{22}^*]^{1/4}}\frac{\bar{W}}{h} + \Theta_1\right] \tag{B.7}$$

in Eq. (B.7) as well as in Eq. (8), the reduced stiffness matrices $[A_{ij}^*]$, $[B_{ij}^*]$, $[D_{ij}^*]$, $[E_{ij}^*]$, $[F_{ij}^*]$ and $[H_{ij}^*]$ (i, j = 1, 2, 6) are evaluated by

$$\begin{gathered}\mathbf{A}^* = \mathbf{A}^{-1},\ \mathbf{B}^* = -\mathbf{A}^{-1}\mathbf{B},\ \mathbf{D}^* = \mathbf{D} - \mathbf{B}\mathbf{A}^{-1}\mathbf{B},\\ \mathbf{E}^* = -\mathbf{A}^{-1}\mathbf{E},\ \mathbf{F}^* = \mathbf{F} - \mathbf{E}\mathbf{A}^{-1}\mathbf{B},\ \mathbf{H}^* = \mathbf{H} - \mathbf{E}\mathbf{A}^{-1}\mathbf{E},\end{gathered} \tag{B.8}$$

where the panel stiffnesses A_{ij}, etc., are given as follows

$$\begin{gathered}\left(A_{ij}, B_{ij}, D_{ij}, E_{ij}, F_{ij}, H_{ij}\right)\\ = \sum_{k=1}^{N}\int_{h_{k-1}}^{h_k}(\bar{Q}_{ij})_k(1, Z, Z^2, Z^3, Z^4, Z^6)dZ\\ (i,j = 1,2,6)\end{gathered} \tag{B.9a}$$

$$\begin{gathered}(A_{ij}, D_{ij}, F_{ij}) = \sum_{k=1}^{N}\int_{h_{k-1}}^{h_k}(\bar{Q}_{ij})_k(1, Z^2, Z^4)dZ\\ (i,j = 4,5)\end{gathered} \tag{B.9b}$$

Appendix C

In Eq. (16)

$$\begin{gathered}C_{11} = \frac{g_8}{g_T},\qquad C_{33} = 1 - \frac{g_{05}}{m^2}\varepsilon,\\ \Theta_1 = \frac{\gamma_{24}^2 - \gamma_5^2}{\gamma_{24}}\frac{\gamma_{T2}}{g_T}\lambda_T^{(0)},\\ \Theta_2 = \frac{1}{C_3}\left[\gamma_{14}\gamma_{24}\frac{2m^4n^2\beta^2(1+\mu)}{J_{22}g_{06}}\varepsilon^{-1}\right.\\ \left.-\gamma_{24}\gamma_{14}\frac{m^2n^2\beta^2 g_{11}}{J_{22}} + 2\frac{\gamma_5}{g_8}\delta_x^{(2)} + \frac{\gamma_{24}^2 - \gamma_5^2}{\gamma_{24}}\frac{\gamma_{T2}}{g_T}\lambda_T^{(2)}\right]\end{gathered} \tag{C.1}$$

$$\begin{gathered}\lambda_x^{(0)} = \frac{1}{2}\left\{\frac{\gamma_{24}m^2}{(1+\mu)g_{06}}\varepsilon^{-1} + \gamma_{24}\frac{g_{05} + (1+\mu)g_{07}}{(1+\mu)^2 g_{06}}\right.\\ \left.+\frac{1}{\gamma_{14}(1+\mu)m^2}\left[g_{08} + F_{11} + \gamma_{14}\gamma_{24}\frac{g_{05}}{g_{06}}\frac{(1+\mu)g_{07} - \mu g_{05}}{(1+\mu)^2}\right]\right.\end{gathered} \tag{C.2}$$

$$\begin{gathered}\lambda_x^{(2)} = \frac{1}{2}\left\{\gamma_{14}\gamma_{24}^2\frac{4m^6n^4\beta^4}{J_{22}g_{06}^2}\varepsilon^{-1} + \gamma_{14}\gamma_{24}^2\frac{2m^4n^4\beta^4}{J_{22}g_{06}(1+\mu)}\right.\\ \left[\frac{g_{07}(1+\mu) + (1-\mu)g_{05}}{g_{06}} + g_{12}(1+\mu)^2 - g_{11}\right]\\ -\frac{1}{16}\gamma_{24}g_{13}\frac{(m^4 + 2\gamma_{24}^2n^4\beta^4)}{m^2}(1+2\mu)\varepsilon\\ +\frac{2\gamma_{14}\gamma_{24}^2m^2n^4\beta^4 g_{05}}{J_{22}g_{06}(1+\mu)^2}\left[2g_{14}(1+\mu)^2\right.\\ \left[+\frac{g_{07}(1+\mu) + 2g_{05}}{g_{06}} - \frac{g_{11}}{2}\right]\varepsilon - \mu\frac{2\gamma_{24}m^2n^4\beta^4}{J_{22}g_{06}}\\ \left[g_{08} + F_{11} + \gamma_{14}\gamma_{24}\frac{g_{05}}{g_{06}}\frac{(1+\mu)g_{07} - \mu g_{05}}{(1+\mu)^2}\right]\varepsilon\\ \left.-\gamma_{14}\gamma_{24}^2\frac{m^2n^4\beta^4 g_{11}g_{12}}{J_{22}}\varepsilon\right\}\end{gathered} \tag{C.3}$$

$$\lambda_x^{(4)} = \frac{1}{2}\left\{\gamma_{14}^2\gamma_{24}^3\frac{4m^{10}n^8\beta^8(1+\mu)}{J_{22}^2g_{06}^3}\frac{S_3}{S_{13}}\varepsilon^{-1}\right\} \tag{C.4}$$

$$\delta_x^{(2)} = \frac{1}{16}\left[(m^2 + \gamma_5n^2\beta^2)(1+2\mu)\varepsilon - 2g_{05}\varepsilon^2 + \frac{g_{05}^2}{m^2}\varepsilon^3\right] \tag{C.5}$$

$$\begin{gathered}\delta_x^{(4)} = \frac{1}{128}\left\{\frac{b_{11}}{\pi\vartheta}\gamma_{14}^2\gamma_{24}^2\frac{8m^8n^4\beta^4(1+\mu)^2}{J_{22}^2g_{06}^2}\varepsilon^{-\frac{3}{2}}\right.\\ \left.+64\gamma_5\gamma_{14}^2\gamma_{24}\frac{m^8n^6\beta^6(1+\mu)^2}{J_{22}^2g_{06}^2}\varepsilon^{-1}\right\}\end{gathered} \tag{C.6}$$

$$\begin{gathered}\lambda_T^{(0)} = 2\lambda_x^{(0)},\quad \lambda_T^{(2)} = 2\lambda_x^{(2)} - 2\frac{\gamma_{24}}{g_8}\delta_x^{(2)},\\ \lambda_T^{(4)} = 2\lambda_x^{(4)} + 2\frac{\gamma_{24}}{g_8}\delta_x^{(4)}\end{gathered} \tag{C.7}$$

All symbols used in the above equations may be found in Shen (2017).